

Relativistic theory for the elementary process of bremsstrahlung induced by heavy spin-zero nuclei

D. H. Jakubassa-Amundsen

Mathematics Institute, University of Munich, Theresienstrasse 39, 80333 Munich, Germany

(Received 27 January 2016; published 27 May 2016)

Doubly and triply differential cross sections for the bremsstrahlung emission by high-energy spin-polarized electrons in the field of heavy bare nuclei are calculated within a fully relativistic partial-wave approach at collision energies between 1 and 30 MeV. Investigating ^{208}Pb as a test case, it is shown that if the photons are emitted at backward angles, nuclear size effects may play an important role even below 10 MeV. Comparison is made with experimental data on the circular polarization correlations between incoming electron and emitted photon at a collision energy of 3.5 MeV. It is demonstrated that, independent of energy, the plane-wave Born approximation severely underestimates the cross section for heavy targets. Moreover, it gives at most a qualitative prescription of the polarization correlations, except possibly in the forward hemisphere.

DOI: [10.1103/PhysRevA.93.052716](https://doi.org/10.1103/PhysRevA.93.052716)**I. INTRODUCTION**

The elementary $(e, e'\gamma)$ process of bremsstrahlung is one of the fundamental electromagnetic processes in electron-atom and electron-nucleus collisions and has been studied for decades, both experimentally and theoretically [1]. As concerns the experiments, the polarization correlations between the incoming electron and the emitted photon were usually measured at collision energies well below 1 MeV. For the $(e, e'\gamma)$ process only the perpendicular spin asymmetry was obtained [1,2], while the other polarization correlations pertaining to linearly polarized photons were basically measured in single (e, γ) experiments [3–5]. Current investigations concern the measurement of the polarization correlations for linearly polarized photons at 2.1 MeV [6] and for circularly polarized photons at 3.5 MeV [7,8]. Due to the recent advances of polarimetry [5,7,9] bremsstrahlung measurements up to several tens of MeV should be feasible.

There is a significant interest in high-energy bremsstrahlung and its electron-photon polarization correlations. From a theoretical point of view, the polarization of the photon emitted in high-energy collisions serves as a sensitive probe of the relativistic dynamics of a spinning charged particle in strong nuclear fields. The consideration of triply differential cross sections provides a much greater wealth of information than spin asymmetries in the doubly differential cross sections where recent experiments [6] have nicely verified the theoretical predictions. Of experimental interest, on the other hand, is the control of the beam polarization during a measurement. This is not possible by conventional Mott or Møller scattering, but can be done by analyzing the circular polarization of bremsstrahlung produced by the polarized beam [7]. The measurement of this circular polarization can be achieved by means of the polarization correlations [9].

Bremsstrahlung can also be investigated in inverse kinematics. In such experiments bare nuclei or highly stripped heavy atoms are collided with light neutral targets, thereby observing the photons from radiative ionization [10]. There is an accelerator upgrading planned to cover beam energies up to 3 GeV and beyond, using the facility to measure triply differential bremsstrahlung cross sections near the short-wavelength limit [11].

A further interest in high-energy bremsstrahlung is a quantification of its role as background effect in nuclear excitation by electron impact [12,13], where the excitation probabilities are usually obtained from the measured spectra by subtracting a smooth background (see, e.g. [14]). In order to elucidate the influence of bremsstrahlung, coincidence experiments are planned in the near future with a high resolution [15]. In such experiments the photon from the decay of the excited nuclear state is detected simultaneously with the energy-analyzed scattered electron. Up to now, there exists a pilot measurement on the ^{12}C nucleus [16] which is theoretically interpreted in [17]. However, the detected photon may also originate from the elementary process of bremsstrahlung, provided the nuclear decay is into the ground state of an unpolarized nucleus. Therefore, in a theoretical model, the amplitude for the bremsstrahlung process has to be added coherently to the one for the inelastic nuclear process [18].

For light and medium target nuclei high-energy bremsstrahlung is conventionally described in terms of the plane-wave Born approximation (PWBA). In this theory the nuclear effects such as finite nuclear size or magnetic moment distribution are incorporated into the Bethe-Heitler model [19] by means of form factors [20]. However, as known from investigations on heavy nuclei at energies below 1 MeV, there are considerable discrepancies in the triply differential cross section between the PWBA and the relativistic partial-wave analysis [21]. In fact, there may even be some discrepancies for medium nuclei like Ag [22]. Another theory which can easily be evaluated in the high-energy regime is the Sommerfeld-Maue (SM) model (also known as Elwert-Haug theory [23,24]), where semirelativistic point-nucleus wave functions are used for the electronic scattering states. Although performing better than the PWBA near the short-wavelength limit (SWL), it is inferior to the relativistic partial-wave prescription for the heavier nuclei (see the comparison of triply differential cross sections and polarization correlations in [22,25]). There exists also a hybrid theory for high-energy bremsstrahlung at the SWL, the Dirac-SM (DSM) model [26] where it is used that the Sommerfeld-Maue functions become exact at very high energies. In the DSM model the initial-state electron is described by such a function while the final electron is a Dirac state of zero kinetic energy. This model works reasonably well near and above 10 MeV [27], but

poor convergence of the two-dimensional radiation integrals prohibits its application beyond 20 MeV.

The most elaborate model existing so far, which is exact for bare nuclei within the one-photon approximation, uses Dirac partial waves for both the electronic scattering states. Such a fully relativistic prescription, including polarization effects, was pioneered by Brysk *et al.* [28], advanced by Tseng and Pratt [22,29], and recently taken up by Yerokhin and co-workers [30,31]. However, because of severe convergence problems of the partial-wave series at the higher energies, this theory has mostly been evaluated at collision energies not exceeding 5 MeV (see also [27,32]). Beyond that there exists a partial-wave interpolation method for the cross section evaluated at 2–10 MeV [33], and a singular partial-wave result at 10 MeV at the SWL [34].

In the present work we set a benchmark by using the standard relativistic partial-wave theory for bremsstrahlung from heavy nuclei, while refining the previously developed procedures in order to cover much higher collision energies. Both doubly and triply differential cross sections as well as the respective polarization correlations are considered. An optimized code for this theory is set up in order to allow predictions for collision energies up to 30 MeV. This covers the region where measurements of the polarization correlations are feasible. We restrict ourselves to the emission of hard circularly polarized photons which are investigated in the ongoing experiments [8]. As concerns the elementary process of bremsstrahlung, our results provide a supplement to the theoretical study of linear polarization correlations in [31]. From experimental and theoretical investigations of the polarization correlations for elastic electron scattering from heavy nuclei [35], as well as from a comparison between the PWBA and the Bethe-Heitler theory for medium-nuclei bremsstrahlung [36], it is evident that at high collision energies there will be appreciable nuclear size effects for nuclei such as ^{208}Pb . Up to now the role of these effects in the triply differential bremsstrahlung cross section for heavy targets was only investigated (within the Dirac theory) for an energy of 0.3 MeV, where they were found to be well below one percent [37].

It is the aim of our investigations to quantify the influence of nuclear size effects and to clarify the validity of the PWBA where it has not been tested before. Also the correspondence in the circular polarization correlations between a hard photon and an elastically scattered electron [38] is extended into the high-energy regime. Moreover, it will be shown how the relativistic focusing changes the angular distribution of both cross sections and spin asymmetries as compared to the low-energy results.

The paper is organized as follows. In Sec. II an outline of the relativistic bremsstrahlung theory is given, adapting the formulation in order to account for spin polarization in a straightforward way. This is followed by the numerical details (Sec. III). Section IV provides results for the circular polarization correlations in a collision geometry where the scattered electron is not observed. Comparison is made with preliminary experimental data at 3.5 MeV. Section V gives predictions for the elementary process of bremsstrahlung. The conclusion is drawn in Sec. VI. Atomic units ($\hbar = m = e = 1$) are used unless indicated otherwise. In particular, the electron mass is retained in all calculations.

II. RELATIVISTIC BREMSSTRAHLUNG THEORY

We restrict ourselves to electron scattering from (bare) spin-zero nuclei which are supposed to remain in their ground state, such that magnetic scattering as well as the dynamical recoil (nuclear bremsstrahlung) is not present. We also assume that the spin polarization of the scattered electron is not observed.

Due to the finite mass M_T of the nucleus kinematical recoil effects are present [39]. Following the emission of a photon with momentum \mathbf{k} and frequency $\omega = kc$ the nucleus recoils with momentum $\mathbf{q} = \mathbf{k}_i - \mathbf{k}_f - \mathbf{k}$ where \mathbf{k}_i and \mathbf{k}_f are the electron momenta in the initial, respectively final, state. As shown in [36] from the conservation of the four-momentum, the energy $E_f = \sqrt{k_f^2 c^2 + c^4}$ of the scattered electron is slightly smaller than the value $E_i - \omega$ resulting from the limit $M_T \rightarrow \infty$. Of course the relations for the four-momentum can also be used to calculate ω for a given E_f .

The triply differential cross section for the emission of bremsstrahlung with polarization \mathbf{e}_λ into the solid angle $d\Omega_k$ by an electron with initial spin vector $\boldsymbol{\zeta}_i$ (and spin projection σ_i), which is scattered into the solid angle $d\Omega_f$, is given by [22]

$$\frac{d^3\sigma}{d\omega d\Omega_k d\Omega_f}(\boldsymbol{\zeta}_i, \mathbf{e}_\lambda) = \frac{4\pi^2 \omega k_f E_f}{c^3 v f_{\text{re}}} \sum_{\sigma_f} |\mathbf{e}_\lambda^* \mathbf{W}_{\text{rad}}(\sigma_f, \sigma_i)|^2, \quad (2.1)$$

where $v = k_i c^2 / E_i$ is the collision velocity, and it is summed over the two spin states σ_f of the scattered electron. f_{re} is a recoil factor [36,39],

$$f_{\text{re}} = 1 - \frac{\mathbf{k}_f \mathbf{q} E_f}{k_f^2 E_{\text{nuc},f}}, \quad (2.2)$$

where $E_{\text{nuc},f} = \sqrt{q^2 c^2 + M_T^2 c^4}$ is the final energy of the nucleus.

The radiation matrix element is given by

$$\mathbf{W}_{\text{rad}}(\sigma_f, \sigma_i) = \int d\mathbf{r} \psi_f^{(\sigma_f)+}(\mathbf{r}) \boldsymbol{\alpha} e^{-i\mathbf{k}\mathbf{r}} \psi_i^{(\sigma_i)}(\mathbf{r}), \quad (2.3)$$

where $\boldsymbol{\alpha}$ is a vector of Dirac matrices, and the electronic scattering states are solutions to the Dirac equation for an arbitrary nuclear potential $V(r)$ [40,41]. For nuclei such as ^{208}Pb , $V(r)$ can be obtained from a Fourier-Bessel expansion of the nuclear ground-state charge density [42].

The wave function of the scattered electron is partial-wave expanded [22,43], taking explicitly account of the spin polarization vector $\boldsymbol{\zeta}_f$,

$$\begin{aligned} \psi_f^{(\sigma_f)+}(\mathbf{r}) &= \sum_{m_s = \pm \frac{1}{2}} b_{m_s}^{(f)*} \sum_{\kappa_f m_f} \left(l_f m_f - m_s \frac{1}{2} m_s |j_f m_f \right) \\ &\times (-i)^{l_f} e^{i\delta_{\kappa_f}} Y_{l_f, m_f - m_s}(\hat{\mathbf{k}}_f) \psi_{\kappa_f m_f}^+(\mathbf{r}), \end{aligned} \quad (2.4)$$

$\psi_{\kappa_f m_f}(\mathbf{r}) = \begin{pmatrix} g_{\kappa_f}(r) Y_{j_f l_f m_f}(\hat{\mathbf{r}}) \\ i f_{\kappa_f}(r) Y_{j_f l'_f m_f}(\hat{\mathbf{r}}) \end{pmatrix}$. The coefficients b_{m_s} are determined by the spherical coordinates of $\boldsymbol{\zeta} = (1, \alpha_s, \varphi_s)$ according to [43]

$$b_{1/2} = \cos \frac{\alpha_s}{2} e^{-i\varphi_s/2}, \quad b_{-1/2} = \sin \frac{\alpha_s}{2} e^{i\varphi_s/2}. \quad (2.5)$$

With the choice of the final polarization along the quantization (z) axis, i.e., $\varphi_s = 0$ and $\alpha_s \in \{0, \pi\}$, one has $b_{m_s}^{(f)} \in \{0, 1\}$.

Below (2.4) g_{κ_f} and f_{κ_f} are, respectively, the large and small components of the radial Dirac functions and Y_{lm} is a spherical harmonic spinor. Furthermore, δ_{κ_f} is the (Coulomb plus short-range) phase shift, $(\cdot \cdot \cdot)$ is a Clebsch-Gordan coefficient, and Y_{lm} a spherical harmonic function as defined in [44].

If one introduces transition amplitudes \mathbf{F}_{fi} by means of

$$\mathbf{W}_{\text{rad}}(\sigma_f, \sigma_i) = \sum_{m_s = \pm \frac{1}{2}} b_{m_s}^{(f)*} \mathbf{F}_{fi}(m_s, \sigma_i), \quad (2.6)$$

the summation over the final spin states is easily carried out,

$$\sum_{\sigma_f} |e_{\lambda}^* \mathbf{W}_{\text{rad}}(\sigma_f, \sigma_i)|^2 = \left| e_{\lambda}^* \mathbf{F}_{fi} \left(\frac{1}{2}, \sigma_i \right) \right|^2 + \left| e_{\lambda}^* \mathbf{F}_{fi} \left(-\frac{1}{2}, \sigma_i \right) \right|^2. \quad (2.7)$$

In order to allow for a convergence acceleration it is of advantage to sum over the angular quantum numbers l_f, j_f and $m_l = m_f - m_s$ in the calculation of \mathbf{F}_{fi} , instead of summing over κ_f and m_f . Then

$$\mathbf{F}_{fi}(m_s, \sigma_i) = \sum_{l_f m_l} Y_{l_f m_l}(\hat{\mathbf{k}}_f) \mathbf{d}_{l_f, m_l}, \quad (2.8)$$

with

$$\mathbf{d}_{l_f, m_l} = (-i)^{l_f} \sum_{j_f} \left(l_f m_l \frac{1}{2} m_s | j_f m_f \right) e^{i\delta_{\kappa_f}} \times \int d\mathbf{r} \psi_{\kappa_f m_f}^+(\mathbf{r}) \boldsymbol{\alpha} e^{-i\mathbf{k}\mathbf{r}} \psi_i^{(\sigma_i)}(\mathbf{r}), \quad (2.9)$$

where $\kappa_f = l_f$ (for $j_f = l_f - \frac{1}{2}$), respectively, $\kappa_f = -l_f - 1$ (for $j_f = l_f + \frac{1}{2}$).

For the initial-state wave function $\psi_i^{(\sigma_i)}$ an expansion similar to (2.4) holds which simplifies considerably when the z axis is taken along \mathbf{k}_i (in contrast to taking it along \mathbf{k} as done in [22]). Upon expanding $e^{-i\mathbf{k}\mathbf{r}}$ in (2.9) in terms of spherical harmonic functions [44], all angular integrals can be performed analytically (see, e.g. [30,40]).

If the scattered electron is not observed, the triply differential cross section (2.1) has to be integrated over the solid angle $d\Omega_f$ of the scattered electron. This is a formidable task because, for a given photon frequency, recoil effects lead to a dependence of the electron energy on the direction $\hat{\mathbf{k}}_f$ of electron emission [45]. However, as discussed below, the omission of recoil is well justified for the heavier spin-zero nuclei, provided the collision energy is not too high and the photons hard (which is the present case of interest). Therefore, recoil is neglected in the doubly differential cross section, upon which the angular integral becomes trivial within the partial-wave representation (2.4),

$$\begin{aligned} & \frac{d^2\sigma}{d\omega d\Omega_k}(\xi_i, \mathbf{e}_{\lambda}) \\ &= \int d\Omega_f \frac{d^3\sigma}{d\omega d\Omega_k d\Omega_f}(\xi_i, \mathbf{e}_{\lambda}) \\ &= \frac{4\pi^2 \omega k_f E_f}{c^3 v} \sum_{\kappa_f m_f} \left| \int d\mathbf{r} \psi_{\kappa_f m_f}^+(\mathbf{r}) (e_{\lambda}^* \boldsymbol{\alpha}) e^{-i\mathbf{k}\mathbf{r}} \psi_i^{(\sigma_i)}(\mathbf{r}) \right|^2. \end{aligned} \quad (2.10)$$

This involves the same integral as occurs in (2.9). However, in (2.10) the final partial waves enter incoherently.

For circularly polarized photons the triply differential cross section (2.1) can be parametrized in terms of the electron-photon polarization correlations $C_{\mu\nu 0}$ in the following way [22],

$$\begin{aligned} & \frac{d^3\sigma}{d\omega d\Omega_k d\Omega_f}(\xi_i, \mathbf{e}_{\pm}) \\ &= \frac{1}{2} \left(\frac{d^3\sigma}{d\omega d\Omega_k d\Omega_f} \right)_0 [1 + \xi_2 C_{020} \\ & \quad - (\xi_i \cdot \mathbf{e}_x)(C_{100} + \xi_2 C_{120}) - (\xi_i \cdot \mathbf{e}_y)(C_{200} + \xi_2 C_{220}) \\ & \quad + (\xi_i \cdot \mathbf{e}_z)(C_{300} + \xi_2 C_{320})], \end{aligned} \quad (2.11)$$

where $\xi_2 = +1$ for a right-handed photon ($\mathbf{e}^{(+)}$) and $\xi_2 = -1$ for $\mathbf{e}^{(-)}$. The first two terms refer to initially unpolarized electrons while the remaining terms correspond to the three Cartesian components of the polarization vector ξ_i [where $\mathbf{e}_z = \hat{\mathbf{k}}_i$, $\mathbf{e}_y = \hat{\mathbf{k}}_i \times \hat{\mathbf{k}}$ with $\hat{\mathbf{k}} = (\sin\theta_k, 0, \cos\theta_k)$ and $\mathbf{e}_x = \mathbf{e}_y \times \hat{\mathbf{k}}_i$]. The prefactor denotes the cross section for unpolarized particles. In coplanar geometry (where \mathbf{k}_f lies in the reaction plane which is spanned by \mathbf{k}_i and \mathbf{k}) it was shown that the parameters C_{020} , C_{100} , C_{220} , and C_{300} vanish [22]. We have verified that these circular polarization correlations also vanish in the general case. If, in addition, ξ_i is chosen in the reaction plane ($\varphi_s = 0$) as done in the experiments on circularly polarized photons [7,8], only C_{120} and C_{320} are accessible. They are obtained by means of the relative cross section differences,

$$\begin{aligned} P_3(\alpha_s) &\equiv \frac{d^3\sigma(\xi_i, \mathbf{e}_+) - d^3\sigma(\xi_i, \mathbf{e}_-)}{d^3\sigma(\xi_i, \mathbf{e}_+) + d^3\sigma(\xi_i, \mathbf{e}_-)} \\ &= C_{320} \cos \alpha_s - C_{120} \sin \alpha_s, \end{aligned} \quad (2.12)$$

with α_s the polar angle of ξ_i . If, on the other hand, ξ_i is perpendicular to the reaction plane ($\alpha_s = \pi/2$, $\varphi_s = -\pi/2$), C_{200} is singled out, which is independent of the photon polarization and mirrors the cross-section asymmetry upon spin flip,

$$C_{200} = \frac{\sum_{\lambda} d^3\sigma(\xi_i, \mathbf{e}_{\lambda}) - \sum_{\lambda} d^3\sigma(-\xi_i, \mathbf{e}_{\lambda})}{\sum_{\lambda} d^3\sigma(\xi_i, \mathbf{e}_{\lambda}) + \sum_{\lambda} d^3\sigma(-\xi_i, \mathbf{e}_{\lambda})}. \quad (2.13)$$

For unobserved electrons the corresponding parametrization reads [29,38]

$$\begin{aligned} & \frac{d^2\sigma}{d\omega d\Omega_k}(\xi_i, \mathbf{e}_{\pm}) = \frac{1}{2} \left(\frac{d^2\sigma}{d\omega d\Omega_k} \right)_0 [1 - \xi_2 C_{12}(\xi_i \cdot \mathbf{e}_x) \\ & \quad - C_{20}(\xi_i \cdot \mathbf{e}_y) + \xi_2 C_{32}(\xi_i \cdot \mathbf{e}_z)], \end{aligned} \quad (2.14)$$

such that (2.12) and (2.13) hold also for the doubly differential cross section (upon replacing $C_{\mu\nu 0}$ by $C_{\mu\nu}$).

III. NUMERICAL DETAILS

The main task is the evaluation of the radial integrals $R(l)$ which are strongly oscillating at large r . In order to cope with this difficulty the complex-plane rotation method (CRM) was introduced in [46] and applied to bremsstrahlung in [30].

The CRM consists in integrating up to a finite distance R_m , well outside the nuclear charge distribution, and deforming the remaining integration path into the complex plane. The CRM was recently adapted to account for a finite nuclear charge distribution in the electronic functions [45], which is used here for the lower partial waves ($|\kappa| \lesssim 100$). Noting that the spherical Bessel functions j_l are real for real arguments, the CRM representation given in [45] simplifies to

$$R_{gf}(l) = \int_0^{R_m} r^2 dr j_l(kr) g_{\kappa_f}(r) f_{\kappa_i}(r) + 2 \operatorname{Re} \left\{ i \int_0^{\infty} dy r^2 j_l(kr) g_{\kappa_f}(r) f_{\kappa_i}^{(+)}(r) \right\} \Big|_{r=R_m+iy}, \quad (3.1)$$

where $f_{\kappa_i}^{(+)}$ is that part of f_{κ_i} which at asymptotically large distances behaves like $f_{\kappa_i}^{(+)}(r) \sim e^{i\kappa_i r}$. Exponential overflow for high E_i is handled by splitting the second integral at some distance y_m while keeping in the integrand of the remainder only the contribution $\sim e^{-\Delta k y}$ (with $\Delta k = k_i - k_f - k > 0$) with the slowest decrease in y .

For the higher partial waves the application of an asymptotic expansion of the radial Dirac functions is no longer possible. Instead, use can be made of the fact that for large angular momenta (corresponding to large $|\kappa|$) the electron does not penetrate into the nucleus and hence experiences a pure Coulomb field, $V(r) = -Z_T/r$ with Z_T the nuclear charge number. Then the Dirac functions can be replaced by the regular pointlike Dirac Coulomb waves [47]. These functions are expressed [30] in terms of Whittaker functions $W_{\alpha,\gamma}$ of the second kind where α is a complex number of order unity. For sufficiently large $r > R_m$ and large $\gamma = \sqrt{\kappa^2 - (Z_T/c)^2}$ they can be calculated from their integral representation [[48], Eq. (13.2.5)]. Asymptotically, they behave like $W_{\alpha,\gamma}(z) \sim e^{-z/2}$. The deformation of the integration path of the radial integrals into the complex plane can therefore be done as before.

The complex integral in (3.1) converges nicely, with $y_m \sim 0.02$ a.u. and an upper cutoff $y_{\max} \sim 8/\Delta k \sim 1$ a.u. It should be noted that Δk , being a small difference of large momenta, is strongly affected by the kinematical recoil. In turn, this influences basically the long-range dipole transitions. Since bremsstrahlung involves, however, the superposition of many multipoles, recoil effects can safely be neglected according to our numerical results for ^{208}Pb .

For the representation of the Bessel functions $j_l(z)$ with $z \in \mathbb{C}$, a highly refined library package [49] is mandatory for $l > 100$, since the upward recursion relations are only valid for large arguments ($|z| > l$). For calculating the radial functions g_κ and f_κ , as well as the Dirac Coulomb waves (along the real axis), the Salvat *et al.* Fortran code RADIAL [41] is used. However, for the higher partial waves, the spacing of grid points used in that code should be reduced to $\Delta r \sim 10^{-2} \times 2\pi/\tilde{k}$, where \tilde{k} denotes the initial or final electron momentum. About 500 grid points are sufficient, provided the integral is not started at $r = 0$, but at a small value well inside the nucleus.

The choice of the upper limit R_m is taken differently for $|\kappa_i| \leq 100$ (large enough such that the asymptotic series for the Dirac waves converge) and for $|\kappa_i| > 100$ (such that the

Whittaker integral representation converges). Typically, $R_m \sim 4000$ – 15000 a.u. for the electron energies considered. Unfortunately, for $|\kappa_i| \gtrsim 600$ (corresponding to $E_i \gtrsim 40$ MeV), an appropriate choice of R_m is no longer possible. This defect might be remedied by a highly refined representation of the Dirac Coulomb waves (in a similar way as is done for the complex Bessel functions), which bridges the gap at intermediate distances r .

For collision energies $E_i \lesssim 30$ MeV the remaining problem is the slow convergence of the partial-wave series in κ_i and κ_f . For the evaluation of the sum (2.8) over the final-state quantum numbers, a convergence acceleration, introduced by Yennie *et al.* [50] and extended in [51], is used for the triply differential cross section. However, while such a multiple convergence acceleration is very efficient for nuclear excitation, there is only a slight improvement on the bremsstrahlung polarization correlations if a onefold acceleration is applied. As a rough estimate, $E_i = 5$ MeV requires $|\kappa_i| \lesssim 120$, $E_i = 10$ MeV requires about 200 partial waves, $E_i = 20$ MeV about 350–400, and $E_i = 30$ MeV about 450–500 partial waves. For the final energies under consideration we have used cutoffs extending at most to 50 partial waves. At the larger photon angles (particularly beyond 160°), there may appear oscillations with the cutoff of κ_f or κ_i even at moderate collision energies [see Figs. 4(b) or 6(b) where such oscillations manifest themselves as wiggles in the angular distribution for a fixed cutoff]. For the smallest collision energies, $E_i \lesssim 1.5$ MeV, the analytic functions for pointlike nuclei can be used throughout.

IV. RESULTS FOR THE DOUBLY DIFFERENTIAL CROSS SECTION

We have performed calculations for electrons scattering from an inert ^{208}Pb nucleus ($Z_T = 82$). In general three models are compared: the plane-wave Born approximation (PWBA) for spin-zero nuclei (including nuclear size effects through a multiplicative charge form factor), the relativistic partial-wave theory for pointlike nuclei (DW-point, where the analytic Dirac Coulomb functions are used throughout), and the relativistic partial-wave theory (DW) pertaining to the finite nuclear charge distribution. Our numerical code was tested against the Sommerfeld-Maue (SM) results for $Z_T = 10$ at forward angles and arbitrary collision energies, both for the doubly and triply differential cross sections and for the respective circular polarization correlations. Moreover, it was tested against the partial-wave results from Yerokhin [49] for the ^{208}Pb point-nucleus doubly differential cross section as well as for C_{32} and C_{12} at a collisions energy $E_{i,\text{kin}} = E_i - c^2$ of 3.5 MeV and various photon frequencies. Very good agreement was found except at the backmost and some near-zero photon angles where the cross section (and hence the polarization correlations) starts to oscillate with the number of partial waves included in the sum.

Figure 1 shows the doubly differential bremsstrahlung cross section as a function of collision energy when the ratio $\omega/E_{i,\text{kin}}$ is kept fixed at 0.75, respectively, 0.95. At a forward photon angle ($\theta_k = 21^\circ$) the PWBA is close to the partial-wave theory except at the lowest energies, and nuclear size effects are negligibly small throughout. At the backward angle ($\theta_k = 140^\circ$ where the electrons come closer to the nucleus) the nuclear size

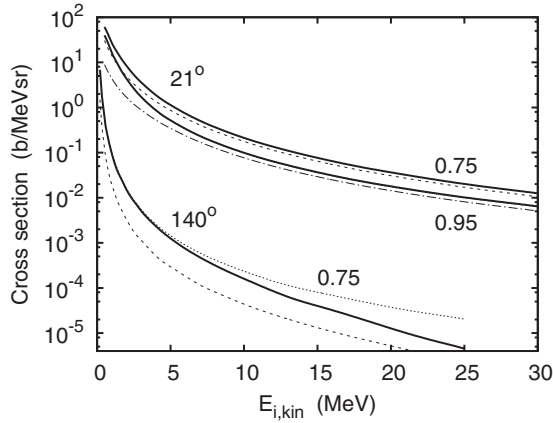


FIG. 1. Doubly differential cross section $d^2\sigma/d\omega d\Omega_k$ for the emission of a photon in the collision with ^{208}Pb as a function of collision energy at an angle $\theta_k = 21^\circ$ (upper curves) and $\theta_k = 140^\circ$ (bottom curves). The photon frequency is $0.75 E_{i,\text{kin}}$ (top and bottom curves) and $0.95 E_{i,\text{kin}}$ (middle curves). Results are shown for the DW theory (—) and for the PWBA [36] (--- for $\omega/E_{i,\text{kin}} = 0.75$; - · - · - for 0.95). Included are results for pointlike nuclei (DW point, ·····). For 21° they are indistinguishable from DW.

effects weaken the Coulomb field and hence lower the cross section considerably, the more so, the higher the energy. The PWBA underestimates the cross section by a factor of 4–5.

In Fig. 2 the corresponding polarization correlations C_{32} and C_{12} are displayed at the forward angle $\theta_k = 21^\circ$. The longitudinal spin asymmetry tends monotonously to zero when $E_{i,\text{kin}} \rightarrow 0$, while C_{12} has a minimum near 2 MeV before increasing to zero. The vanishing of both spin asymmetries in the nonrelativistic limit is a clear signature that polarization transfer is a relativistic effect. At large E_i , C_{32} tends to unity which means that the polarization transfer from a helicity (+) electron to the helicity (+) photon is complete. Since elastically scattered electrons have the same property (i.e., the longitudinal polarization $L \rightarrow 1$ is conserved during the scattering process), a hard photon (near the SWL) may be considered as being equivalent to an electron scattered elastically into the same direction (for sufficiently high collision energies where the electron mass is of minor importance [38]). On the other hand, C_{12} tends to zero with E_i . This behavior is related to a sum rule for elastic scattering [52], which involves the three polarization correlations L, R, S [corresponding to the initial electron spin orientation along one of the coordinate axes in analogy to (2.14)], that is strictly valid for potential scattering ($L^2 + R^2 + S^2 = 1$). In fact, this sum rule is approximately valid for the three circular polarization correlations, i.e., $C_{32}^2 + C_{12}^2 + C_{20}^2 \approx 1$ [38], such that $C_{32} \approx 1$ implies $C_{12} \approx 0$. The negative values of C_{12} can be explained by the fact that for this polarization correlation the initial electron spin ξ_i lies in the opposite half plane (with respect to the beam axis) as the emitted photon, thus preferring polarization transfer to a left-handed photon. The PWBA reproduces the global E_i dependence, but with large deviations at lower energy while gradually coming closer to the partial-wave result at the highest E_i .

Also shown in this figure are preliminary experimental data at 3.5 MeV for a ^{197}Au target ($Z_T = 79$). Magnetic scattering

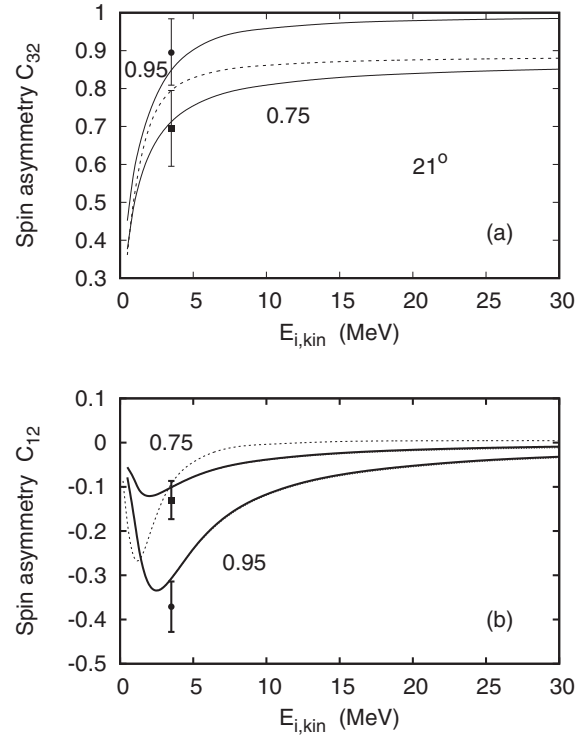


FIG. 2. Spin asymmetries (a) C_{32} and (b) C_{12} for photons emitted at $\theta_k = 21^\circ$ as a function of collision energy. The photon frequency is $0.75 E_{i,\text{kin}}$ [lower curves in (a); upper curves in (b)] and $0.95 E_{i,\text{kin}}$ [top curve in (a); bottom curve in (b)]. Theory for ^{208}Pb : DW (—), PWBA for $\omega = 0.75 E_{i,\text{kin}}$ (---). DW point is indistinguishable from DW. Included are experimental results for 3.5 MeV electrons scattering from an ^{197}Au target: $\theta_k = 21^\circ$, $\omega/E_{i,\text{kin}} = 0.75$ (■) and 0.95 (●) as described in [8].

and dynamical recoil effects are present for this spin $\frac{3}{2}$ target, but are still negligible at 21° for this low energy. In turn, the energy is high enough such that the screening of the gold atom by the atomic electrons plays no role anymore [30]. For comparison we have evaluated the DW theory for gold by using a two-parameter Fermi nuclear charge distribution [42], but neglecting the spin of the nucleus and screening effects. For $E_i = 3.5$ MeV and $\theta_k = 21^\circ$ we have obtained $C_{32} = 0.715$ (versus $C_{32} = 0.712$ for ^{208}Pb) and $C_{12} = -0.105$ (versus -0.101) if $\omega/E_{i,\text{kin}} = 0.75$, while $C_{32} = 0.856$ (versus $C_{32} = 0.848$ for ^{208}Pb) and $C_{12} = -0.308$ (versus -0.307) if $\omega/E_{i,\text{kin}} = 0.95$. This is a deviation of 3.5% or less between the two targets which cannot be distinguished within the experimental accuracy.

Figure 3 provides the spin asymmetry for 140° . The global energy dependence is basically similar to that for forward angles. However, C_{32} now also exhibits a negative minimum at the smallest energies before tending to zero. The transition from a monotonous decrease of C_{32} to zero to an oscillatory behavior occurs around an angle of 80° . The negativity of C_{32} at small energy but large angles again correlates to the behavior of the spin transfer during elastic electron scattering: the drop with angle from $L = 1$ to $L = -1$ occurs the earlier, the smaller E_i [38,52], such that at large enough angles, the spin asymmetry is negative for small collision energies and positive

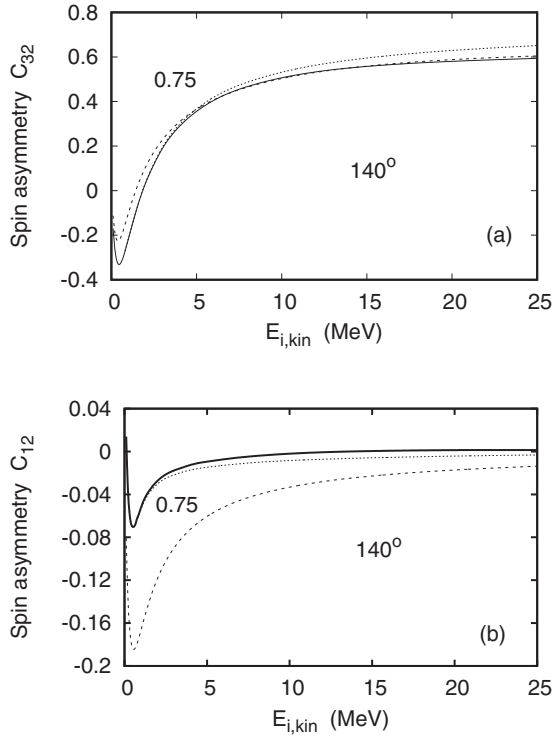


FIG. 3. Spin asymmetries (a) C_{32} and (b) C_{12} for photons emitted in the collision with ^{208}Pb at $\theta_k = 140^\circ$ with frequency $0.75 E_{i,\text{kin}}$ as a function of collision energy. Results are shown for DW (—), for PWBA (---), and DW point (·····).

for large E_i . Moreover, nuclear size effects are present already well below 10 MeV, particularly for the small polarization correlation C_{12} . It should be noted that the PWBA does not account for nuclear size effects in the spin asymmetries since, according to (2.12), they are obtained from the relative cross section differences where the nuclear form factor drops out.

For the sake of completeness we have included a result for the perpendicular spin asymmetry $A = C_{20}$ which vanishes in PWBA [1,29]. In order to compare with other higher-order theories such as the DSM we consider in Fig. 4 the short-wavelength limit, $\omega \approx E_i - c^2 = 10$ MeV. It is seen that the DSM provides a qualitative description of the angular distribution, being much closer to the DW theory than to the DW point (even more so when $E_{i,\text{kin}}$ is increased to 15 MeV). This result may be explained by a comparable reduction of the influence of the Coulomb field in the finite-nuclear-size functions as well as in the semirelativistic SM functions at small r . Moreover, the DSM cross section is at large θ_k even below the SM result. This reduction may be caused by a mismatch (at small r) of the two different electronic functions used in the DSM theory. The spin asymmetry A , shown in Fig. 4(b), exhibits a large peak at the backmost angles which is strongly enhanced if nuclear size effects are taken into account. This enhancement by screening effects, which is also known from low-energy investigations [29], may tentatively be explained by the polarizability response of a charged sphere that is correlated with the direction of ζ_i and hence causes a strong cross-section asymmetry. The SM theory does not predict the narrow peak of A which, due to the high momentum

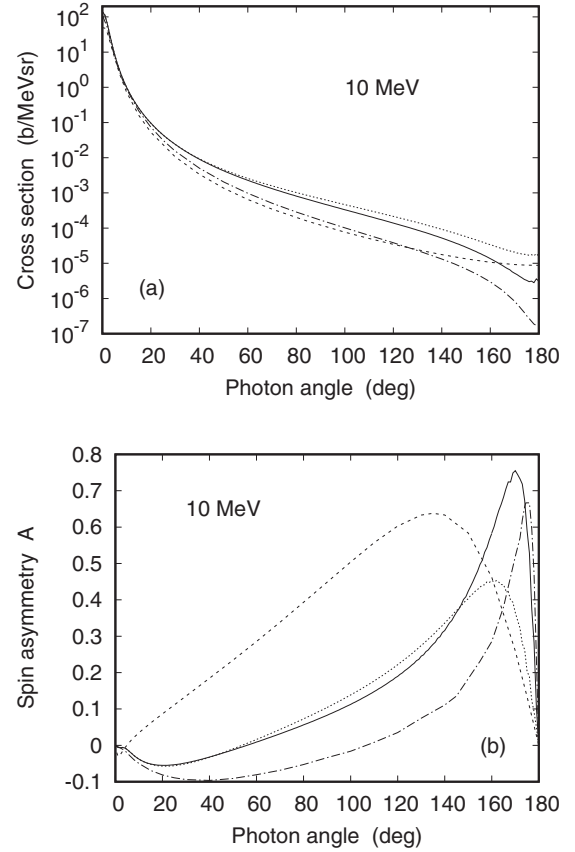


FIG. 4. (a) Doubly differential cross section $d^2\sigma/d\omega d\Omega_k$ and (b) spin asymmetry A from 10 MeV electrons colliding with ^{208}Pb as a function of photon emission angle θ_k . Results for $\omega = 9.9$ MeV are shown using DW (—), DW point (·····), and SM (---). The DSM results (— · — ·) are for $\omega = 10$ MeV.

transfer, mirrors the relativistic contraction of the electronic wave function that is absent in SM. In fact, the failure of the SM model for the polarization correlations of heavy atoms is a general feature.

V. RESULTS FOR THE ELEMENTARY PROCESS OF BREMSSTRAHLUNG

A more detailed access to the scattering process is attained by observing the bremsstrahlung photons in coincidence with the inelastically scattered electrons. The information is provided by the triply differential cross section and the corresponding electron-photon polarization correlations. One might go into further detail by investigating in addition the polarization correlations between ingoing and scattered electron or between the photon and the scattered electron as indicated in [1]. This is not done here, but can easily be achieved within the formalism of Sec. II by omitting the sum over σ_f in (2.1).

We start by giving an overview over the photon angular dependence of the triply differential cross section in coplanar geometry (where the azimuthal angle φ of the electron with respect to the photon is either set to zero or to 180°). Since the variation with collision energy is moderate in this high-energy region, both for the cross section and for the polarization

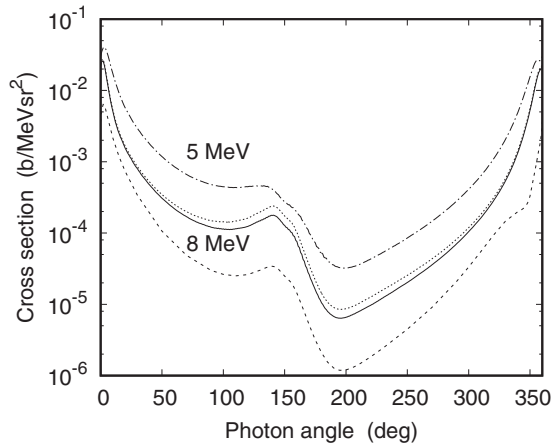


FIG. 5. Triply differential cross section $d^3\sigma/d\omega d\Omega_k d\Omega_f$ for the emission of a 6 MeV photon from 8 MeV electrons colliding with ^{208}Pb as a function of photon angle θ_k at a scattering angle $\vartheta_f = 150^\circ$ (with $\varphi = 0$). Results are shown for DW (—), PWBA (---), and DW point (·····). Included are DW results at 5 MeV, $\omega/E_{i,\text{kin}} = 0.75$, and $\vartheta_f = 150^\circ$ (-·-·-·).

correlations, we have in Fig. 5 chosen an energy of 8 MeV and a photon frequency of 6 MeV. At such energies the cross section peaks near $\theta_k = 0$ and has a minimum near 180° . However, for nonzero (and not too small) electron angles there is, in contrast to the doubly differential cross section [Fig. 4(a)], no longer a monotonous decrease with θ_k . Instead, for a backward scattered electron with $\vartheta_f = 150^\circ$ as selected in the figure, the cross section has a local maximum near 150° ($\theta_k = \vartheta_f$). Also the symmetry with respect to $\theta_k = 180^\circ$ is broken when ϑ_f is moved away from 0 or π . The fact that the photon and electron are preferably emitted into the same direction (and not, symmetrical to the beam axis, into different half-planes which would correspond to $\theta_k = 2\pi - \vartheta_f$) is well known from observations below 1 MeV [1,25]. The PWBA provides only a minor fraction of the cross section, irrespective of the photon angle. The reason lies in the fact that the plane waves do not account for rescattering from the nuclear potential in contrast to the Dirac waves. Therefore, the intensity of the backscattered electrons is severely underestimated. Nuclear size effects are moderate at this energy, being strongest at the backward photon angles. Included in the figure is the result for 5 MeV electrons and 3.75 MeV photons. The photon intensity is higher, but the angular distribution is basically the same as for 8 MeV. Only the peak at $\theta_k = \vartheta_f$ is less prominent than for the higher collision energy.

Figure 6 displays the angular dependence of the corresponding polarization correlations. The longitudinal spin asymmetry C_{320} , shown in Fig. 6(a), drops irrespective of ϑ_f from near unity to -1 at angles up to 180° , and the falloff is shifted to larger θ_k for higher E_i . This behavior corresponds to the one known from C_{32} where the electron remains unobserved. There is, however, an additional small hump near $\theta_k = \vartheta_f$ in this angular dependence, and this hump becomes more visible when the collision energy increases.

A striking feature is the resonantlike structure of C_{120} [Fig. 6(b)] near the local maximum of the cross section (with values close to zero at $\theta_k = 150^\circ$). If ϑ_f is lowered, the

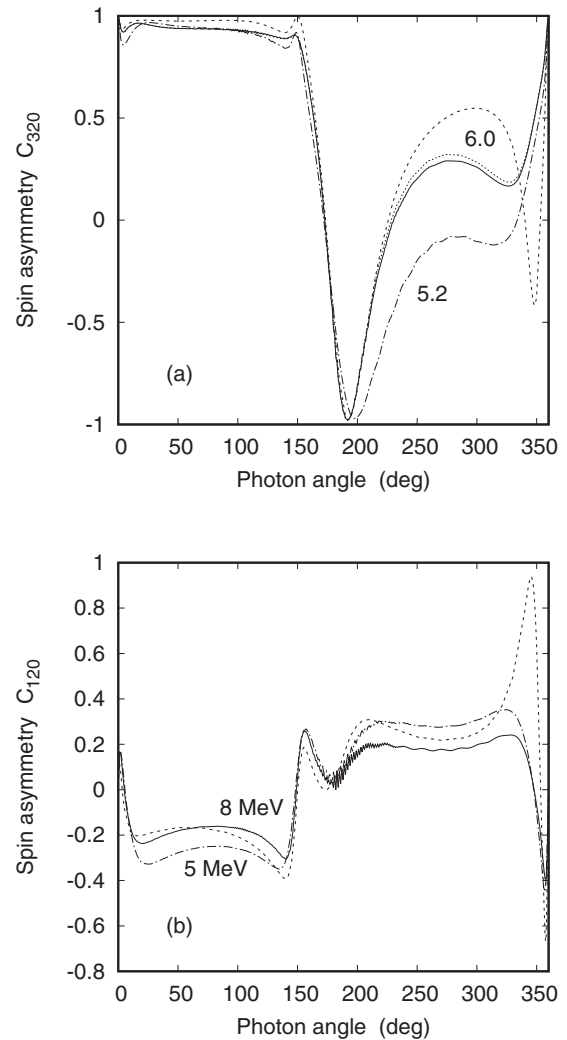


FIG. 6. Spin asymmetries (a) C_{320} and (b) C_{120} from the emission of a 6 MeV photon by 8 MeV electrons colliding with ^{208}Pb as a function of photon angle θ_k at a scattering angle $\vartheta_f = 150^\circ$ (and $\varphi = 0$). Results are shown for DW (—), PWBA (---), and DW point [·····, only shown in (a)]. Included are DW results for C_{120} at 5 MeV ($\omega = 3.75$ MeV, -·-·-·) and for C_{320} at 8 MeV but $\omega = 5.2$ MeV (-·-·-·), all for $\vartheta_f = 150^\circ$.

structure moves accordingly to smaller photon angles, while the shape of C_{120} beyond 180° is not much affected. In the case where the electron is not detected, the angular distribution of the respective spin asymmetry C_{12} resembles the one of C_{120} for large ϑ_f , but with a simple rise to zero beyond the minimum [38] in the region 160° – 180° .

When the photon frequency is decreased [see, e.g., Fig. 6(a)] the structures become narrower and more enhanced, but the angular distribution remains similar. In the PWBA the spin asymmetries are reasonably well described up to $\theta_k \sim 180^\circ$, but this theory strongly overestimates the second structure near 350° – 360° , which corresponds to the main maximum of the cross section.

For investigating the collision energy dependence of the triply differential cross section and the corresponding polarization correlations we consider in the following three particular

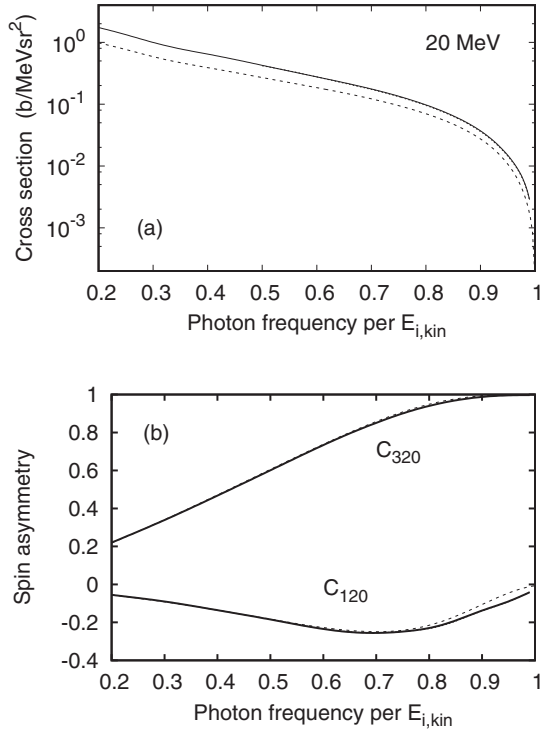


FIG. 7. Dependence (a) of the triply differential cross section and (b) of the spin asymmetry on the ratio $\omega/E_{i,\text{kin}}$ for 20 MeV electrons colliding with ^{208}Pb . The angles are $\theta_k = 20^\circ$ and $\vartheta_f = 25^\circ$ ($\varphi = 0$). Results are shown for DW (—) and PWBA (---). DW point is indistinguishable from DW.

cases: (a) where both electron and photon are emitted close to each other in the forward direction, (b) when they are emitted back-to-back close to the beam axis, and (c) when both particles are emitted into the backward direction. Such geometries are chosen because there the corresponding spin asymmetries have local extrema.

In these investigations the ratio $\omega/E_{i,\text{kin}}$ between the photon frequency and the electron impact energy is again kept fixed. Actually the variation of the cross section and the spin asymmetries with ω is smooth as shown in Fig. 7 for 20 MeV electrons and geometry (a). It is found that the cross section decreases monotonously with frequency, which also holds true when the electron solid angle is integrated over. This feature is reproduced by the PWBA. However, the PWBA fails near the SWL where it predicts cross sections which tend to zero in contrast to the results from a higher-order theory [23,26,30]. Nuclear size effects increase with ω (since harder photons require larger momentum transfers, respectively closer electron-nucleus encounters), but, as before, they are negligible at forward angles.

Figure 7(b) depicts the corresponding spin asymmetries. The longitudinal spin transfer increases with ω and approaches unity at the SWL. This behavior holds also true in the doubly differential case (see, e.g., [7] for 3.5 MeV). On the other hand, the transverse polarization correlation C_{120} has a weak extremum near $\omega = 0.7E_{i,\text{kin}}$ for forward scattering, while an integration over the electron angles leads to a monotonous decrease of C_{12} with ω . The moduli of C_{120} are also much larger than those of C_{12} . For example, for 20 MeV and $\theta_k = 20^\circ$, C_{12}

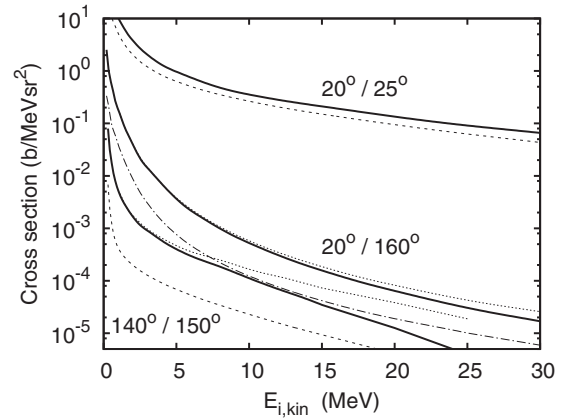


FIG. 8. Triply differential cross section for the emission of a photon with frequency $\omega = 0.75E_{i,\text{kin}}$ in the collision with ^{208}Pb as a function of $E_{i,\text{kin}}$. The angles are $\theta_k = 20^\circ$, $\vartheta_f = 25^\circ$, $\varphi = 0$ (upper curves), $\theta_k = 20^\circ$, $\vartheta_f = 160^\circ$, $\varphi = 180^\circ$ (middle curves), and $\theta_k = 140^\circ$, $\vartheta_f = 150^\circ$, $\varphi = 0$ (bottom curves). Results are shown for DW (—), PWBA (--- for $\vartheta_f = 25^\circ$ and 150° , - · - · - for $\vartheta_f = 160^\circ$), and DW point (·····).

decreases to -0.053 at $\omega = 0.95E_{i,\text{kin}}$, while C_{120} reaches values down to -0.26 for $\vartheta_f = 25^\circ$.

In Figs. 8–10 representatives for the energy dependence in the three collision geometries introduced above are shown. From Fig. 8 it follows that not only the doubly, but also the triply differential cross sections decrease with energy in the energy region considered. This decrease gets steeper when the electron is scattered into backward directions.

Figure 9 shows the corresponding longitudinal polarization correlation C_{320} . While for forward emission C_{320} tends monotonously to zero when $E_{i,\text{kin}} \rightarrow 0$, the backward emission of the two particles leads to a minimum which survives when the electron angle is integrated over (Fig. 3). When the particles are emitted back-to-back ($\theta_k = 20^\circ$, $\vartheta_f = 160^\circ$, $\varphi = 180^\circ$), C_{320} remains positive while oscillating weakly near 3 MeV before tending to zero. Also, in this geometry, C_{320} does not approach unity at large E_i but instead remains approximately constant at a low value [see Fig. 6(a) near 340°].

The energy dependence of the transverse polarization correlation C_{120} is displayed in Fig. 10. Clearly, C_{120} tends to zero for large E_i in a similar way at all angles. However, while the minimum at $E_{i,\text{kin}} < 5$ MeV is quite deep at forward photon angles, both for forward and backward scattering, it is shallower when the two particles are emitted in backward directions. In the latter case there is also a weak second minimum near 0.5 MeV. In that region the PWBA seriously overestimates the magnitude of this spin asymmetry.

VI. CONCLUSION

We have given predictions for the doubly and triply differential bremsstrahlung cross sections and for the respective spin asymmetries within the fully relativistic partial-wave theory for a large variety of collision energies, photon frequencies, and emission angles. At a collision energy of 3.5 MeV and a photon angle of 21° good agreement with preliminary experimental (e, γ) data on the circular polarization correlations

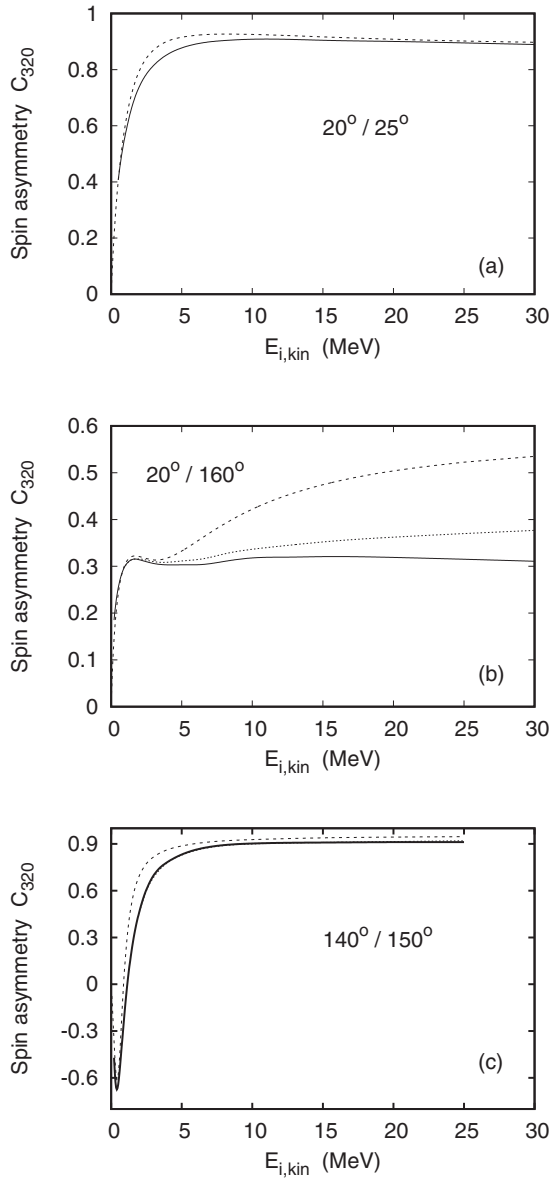


FIG. 9. Spin asymmetry C_{320} for the emission of photons with frequency $\omega = 0.75E_{i,\text{kin}}$ in the collision with ^{208}Pb as a function of $E_{i,\text{kin}}$. The angles are (a) $\theta_k = 20^\circ$, $\vartheta_f = 25^\circ$, $\varphi = 0$, (b) $\theta_k = 20^\circ$, $\vartheta_f = 160^\circ$, $\varphi = 180^\circ$, and (c) $\theta_k = 140^\circ$, $\vartheta_f = 150^\circ$, $\varphi = 0$. Results are shown for DW (—), PWBA (---), and DW point (⋯⋯). In (a) and (c), DW point is indistinguishable from DW.

C_{32} and C_{12} for a gold target was obtained. A systematic study of the energy dependence of the polarization correlations pertaining to the doubly differential cross section reveals maximum moduli of C_{12} and A in the region 3–10 MeV. Beyond, there is a weak variation with E_i until energies where the electron will penetrate the nucleus. Nuclear size effects lead to a considerable reduction of the cross section for wide-angle bremsstrahlung, the more so, the higher E_i , and they also modify A and C_{12} . These two transverse spin asymmetries are thus promising candidates for investigating details of the nuclear structure at the higher energies.

The coincident detection of photon and scattered electron leads to an enhanced occurrence of structures both in the

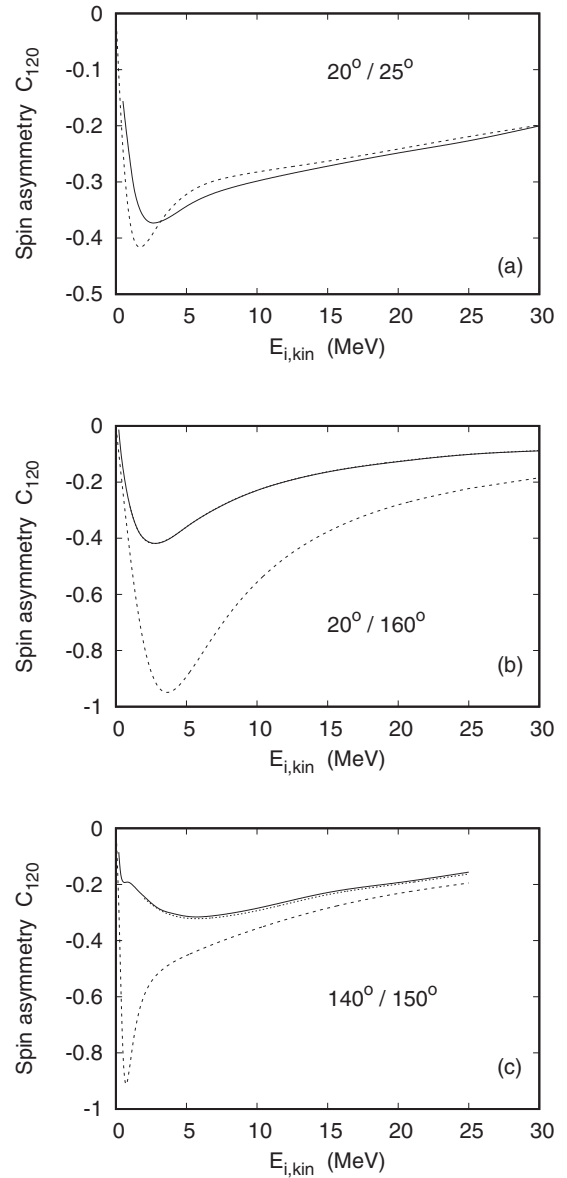


FIG. 10. Spin asymmetry C_{120} for the emission of photons with frequency $\omega = 0.75E_{i,\text{kin}}$ in the collision with ^{208}Pb as a function of $E_{i,\text{kin}}$. The angles are (a) $\theta_k = 20^\circ$, $\vartheta_f = 25^\circ$, $\varphi = 0$, (b) $\theta_k = 20^\circ$, $\vartheta_f = 160^\circ$, $\varphi = 180^\circ$, and (c) $\theta_k = 140^\circ$, $\vartheta_f = 150^\circ$, $\varphi = 0$. Results are shown for DW (—), PWBA (---), and DW point (⋯⋯, only marginally visible in (c)).

cross section and in the spin asymmetries. At the highly relativistic energies considered, the maximum in the cross section occurring when electron and photon are emitted into the same hemisphere [1] dissolves into two peaks. The main peak is near $\theta_k = 0$ (in the beam direction), the other one close to the direction of the scattered electron ($\theta_k = \vartheta_f$), confirming earlier PWBA results [39]. Both peaks are increasingly narrow and prominent when either the initial or the final energy of the electron gets higher. In turn, the polarization correlations show resonance structures in these two angular regimes. These structures are hardly affected by the collision energy, but they are strongly enhanced when the energy of the scattered electron is increased. The longitudinal spin transfer to the photon is

nearly complete at angles below 180° , irrespective of the collision energy or of the detection of the scattered electron. However, C_{12} can attain much larger values if the electron is recorded in coincidence, but it decreases with collision energy.

Again there are considerable nuclear size effects which predominantly affect the cross section. At 10 MeV, they may lead to a reduction by 60% if both particles are emitted into the backward direction, increasing to a factor of 3 at 20 MeV. By comparing with our partial-wave results we have confirmed that the DSM model for the SWL provides a qualitative picture at an energy as low as 10 MeV. However, the PWBA fails for a heavy target, even at high energies, since it does not permit efficient backscattering of the electron. Hence, except at the foremost angles, it cannot be used to make reliable predictions at energies beyond 30 MeV where a partial-wave analysis is no longer possible.

Since restriction was made to the emission of hard photons, requiring large momentum transfers and hence close electron-nucleus encounters, the present high-energy results are also valid if the target carries electrons instead of being a bare nucleus. Atomic screening will modify the displayed results only below, say, 2 MeV, but rather in a quantitative, not in a qualitative way.

ACKNOWLEDGMENTS

It is a pleasure to thank V. A. Yerokhin for his help with specific ingredients of the numerical code, and for performing a series of calculations for testing the code. I would also like to thank K. Aulenbacher and F. Nillius for many enlightening discussions in Mainz and for providing me with experimental data prior to publication.

-
- [1] E. Haug and W. Nakel, *The Elementary Process of Bremsstrahlung* (World Scientific, Singapore, 2004).
- [2] W. Nakel, *Phys. Rep.* **243**, 317 (1994).
- [3] S. Tashenov, T. Bäck, R. Barday, B. Cederwall, J. Enders, A. Khaplanov, Yu. Poltoratska, K.-U. Schässburger, and A. Surzhykov, *Phys. Rev. Lett.* **107**, 173201 (2011).
- [4] R. Märtin, G. Weber, R. Barday, Y. Fritzsche, U. Spillmann, W. Chen, R. D. DuBois, J. Enders, M. Hegewald, S. Hess, A. Surzhykov, D. B. Thorn, S. Trotsenko, M. Wagner, D. F. A. Winters, V. A. Yerokhin, and Th. Stöhlker, *Phys. Rev. Lett.* **108**, 264801 (2012).
- [5] S. Tashenov, T. Bäck, R. Barday, B. Cederwall, J. Enders, A. Khaplanov, Yu. Fritzsche, K.-U. Schässburger, A. Surzhykov, V. A. Yerokhin, and D. Jakubassa-Amundsen, *Phys. Rev. A* **87**, 022707 (2013).
- [6] O. Kovtun, V. Tioukine, A. Surzhykov, V. A. Yerokhin, B. Cederwall, and S. Tashenov, *Phys. Rev. A* **92**, 062707 (2015).
- [7] R. Barday, K. Aulenbacher, P. Bangert, J. Enders, A. Göök, D. H. Jakubassa-Amundsen, F. Nillius, A. Surzhykov, and V. A. Yerokhin, *J. Phys. Conf. Ser.* **298**, 012022 (2011).
- [8] F. Nillius and K. Aulenbacher, Proceedings of Science **PSTP2015**, 031 (2016).
- [9] S. Tashenov, *Nucl. Instrum. Methods Phys. Res., Sect. A* **640**, 164 (2011).
- [10] M. Nofal, S. Hagmann, Th. Stöhlker, D. H. Jakubassa-Amundsen, Ch. Kozhuharov, X. Wang, A. Gumberidze, U. Spillmann, R. Reuschl, S. Hess, S. Trotsenko, D. Banas, F. Bosch, D. Liesen, R. Moshhammer, J. Ullrich, R. Dörner, M. Steck, F. Nolden, P. Beller, H. Rothard, K. Beckert, and B. Franczak, *Phys. Rev. Lett.* **99**, 163201 (2007).
- [11] P.-M. Hillenbrand *et al.*, *Phys. Scr.* **T156**, 014087 (2013).
- [12] L. C. Maximon and D. B. Isabelle, *Phys. Rev.* **133**, B1344 (1964).
- [13] E. S. Ginsberg and R. H. Pratt, *Phys. Rev.* **134**, B773 (1964).
- [14] P. v. Neumann-Cosel *et al.*, *Phys. Rev. Lett.* **82**, 1105 (1999).
- [15] N. Pietralla and P. v. Neumann-Cosel, DFG Proposal for SFB 1245, 2015 (unpublished).
- [16] C. N. Papanicolas, S. E. Williamson, H. Rothhaas, G. O. Bolme, L. J. Koester, Jr., B. L. Miller, R. A. Miskimen, P. E. Mueller, and L. S. Cardman, *Phys. Rev. Lett.* **54**, 26 (1985).
- [17] D. G. Ravenhall, R. L. Schult, J. Wambach, C. N. Papanicolas, and S. E. Williamson, *Ann. Phys. (N.Y.)* **178**, 187 (1987).
- [18] H. L. Acker and M. E. Rose, *Ann. Phys. (NY)* **44**, 336 (1967).
- [19] H. Bethe and W. Heitler, *Proc. R. Soc. London A* **146**, 83 (1934).
- [20] R. A. Berg and C. N. Lindner, *Phys. Rev.* **112**, 2072 (1958).
- [21] C. D. Shaffer and R. H. Pratt, *Phys. Rev. A* **56**, 3653 (1997).
- [22] H. K. Tseng, *J. Phys. B* **35**, 1129 (2002).
- [23] G. Elwert and E. Haug, *Phys. Rev.* **183**, 90 (1969).
- [24] E. Haug, *Z. Phys. D* **37**, 9 (1996).
- [25] C. D. Shaffer, X.-M. Tong, and R. H. Pratt, *Phys. Rev. A* **53**, 4158 (1996).
- [26] D. H. Jakubassa-Amundsen, *Phys. Rev. A* **82**, 042714 (2010).
- [27] D. H. Jakubassa-Amundsen and A. Surzhykov, *Eur. Phys. J. D* **62**, 177 (2011).
- [28] H. Brysk, C. D. Zerby, and S. K. Penny, *Phys. Rev.* **180**, 104 (1969).
- [29] H. K. Tseng and R. H. Pratt, *Phys. Rev. A* **7**, 1502 (1973).
- [30] V. A. Yerokhin and A. Surzhykov, *Phys. Rev. A* **82**, 062702 (2010).
- [31] R. A. Müller, V. A. Yerokhin, and A. Surzhykov, *Phys. Rev. A* **90**, 032707 (2014).
- [32] R. H. Pratt and H. K. Tseng, *Phys. Rev. A* **11**, 1797 (1975).
- [33] H. K. Tseng and R. H. Pratt, *Phys. Rev. A* **19**, 1525 (1979).
- [34] E. Haug, *Eur. Phys. J. D* **58**, 297 (2010).
- [35] J. Sromicki, K. Bodek, D. Conti, St. Kistryn, J. Lang, S. Navert, O. Naviliat-Cuncic, E. Stephan, C. Sys, J. Zejma, W. Haerberli, E. Reichert, and M. Steigerwald, *Phys. Rev. Lett.* **82**, 57 (1999).
- [36] D. H. Jakubassa-Amundsen, *Phys. Rev. C* **87**, 064609 (2013).
- [37] S. Keller and R. M. Dreizler, *J. Phys. B* **30**, 3257 (1997).
- [38] D. H. Jakubassa-Amundsen, *Phys. Rev. A* **85**, 042714 (2012).
- [39] S. D. Drell, *Phys. Rev.* **87**, 753 (1952).
- [40] H. K. Tseng and R. H. Pratt, *Phys. Rev. A* **3**, 100 (1971).
- [41] F. Salvat, J. M. Fernández-Varea, and W. Williamson, Jr., *Comput. Phys. Commun.* **90**, 151 (1995).
- [42] H. De Vries, C. W. De Jager, and C. De Vries, *At. Data Nucl. Data Tables* **36**, 495 (1987).
- [43] M. E. Rose, *Relativistic Electron Theory* (Wiley, New York, 1961).

- [44] A. R. Edmonds, *Angular Momentum in Quantum Mechanics*, 2nd ed. (Princeton University Press, Princeton, NJ, 1960).
- [45] D. H. Jakubassa-Amundsen and V. Yu. Ponomarev, *Eur. Phys. J. A* **52**, 48 (2016).
- [46] C. M. Vincent and H. T. Fortune, *Phys. Rev. C* **2**, 782 (1970).
- [47] V. B. Berestetskii, E. M. Lifshitz, and L. P. Pitaevskii, *Quantum Electrodynamics*, 2nd ed., Course of Theoretical Physics Vol. 4 (Elsevier, Oxford, 1982), §36.
- [48] M. Abramowitz and I. A. Stegun, *Handbook of Mathematical Functions* (Dover Publications, New York, 1964).
- [49] V. A. Yerokhin (private communication).
- [50] D. R. Yennie, D. G. Ravenhall, and R. N. Wilson, *Phys. Rev.* **95**, 500 (1954).
- [51] S. T. Tuan, L. E. Wright, and D. S. Onley, *Nucl. Instrum. Methods* **60**, 70 (1968).
- [52] J. W. Motz, H. Olsen, and H. W. Koch, *Rev. Mod. Phys.* **36**, 881 (1964).